16th World Conference on Earthquake, 16WCEE 2017

Santiago Chile, January 9th to 13th 2017

Paper N°681

Registration Code: S-W1464748284

MODELLING OF RC WALLS WITH DUCTILE DETAILING SUBJECTED TO HIGH AXIAL LOADS

A.S. Shegay[(1)], C.J. Motter[(2)], R.S. Henry[(3)], K.J. Elwood[(4)]

[(1)] *PhD Candidate, University of Auckland, alex.shegay@auckland.ac.nz*
[(2)] *Research Fellow, University of Auckland c.motter@auckland.ac.nz*
[(3)] *Senior Lecturer, University of Auckland, rs.henry@auckland.ac.nz*
[(4)] *Professor, University of Auckland, k.elwood@auckland.ac.nz*

Abstract

Observations following the 2010/2011 Canterbury Earthquakes revealed unexpected damage to reinforced concrete walls, characterized by undesirable failure modes such as crushing of concrete and buckling of longitudinal reinforcement in the web and end regions. In an effort to address these failures, a number of changes have been made to the New Zealand Concrete Structures Standard (NZS3101:2006) that will be published in the next amendment. Major changes include an introduction of an axial load limit ($P \leq 0.3A_g f'_c$) and changes to confinement detailing of the wall web and end regions. Four large-scale walls (C10-A30) are currently being tested to assess the effects that variation of these parameters will have on wall response. Prior to commencing experimental testing, blind predictions have been made using nonlinear finite element models developed in VecTor2. The models were calibrated against test results for five walls with similar detailing and loading conditions to C10-A30. The calibrated models successfully matched strength capacity, failure mode (flexural crushing). Drift at failure observed in experiments was simulated with an average accuracy of 5-30%. Using the modelling approach, C10-A30 were predicted to exhibit generally poor performance characterized by low ductility. Specifically, C10 and A10, with axial load ratios of $0.1A_g f'_c$, were predicted to reach 1.6% and 1.8% drift, respectively, before failure with an average ductility of 3. A longer confinement length in A10 compared to C10 had only a minor effect on the deformation capacity. Specimen A20 (axial load of $0.2A_g f'_c$) and A30 (axial load of $0.3A_g f'_c$) were predicted to reach 1.2% drift and 1.05% drift, respectively, with no ductility due to compression-controlled flexural failure resulting from the large axial loads. Failure was characterized by a rapid loss of strength in a brittle compression failure.

Keywords: RC Walls; high axial load, confinement length; VecTor2.

1. Introduction

The peak ground accelerations produced during the 2011 February earthquake in Christchurch (M_w=6.3) were some of the largest ever recorded in an urbanised area. While most reinforced concrete (RC) wall buildings achieved their life-safety design objective, a number of RC walls were found to have sustained severe and unexpected damage. Undesirable failure modes were observed, including buckling of longitudinal reinforcement and crushing of concrete at the wall end region. Damage reports and design guidelines emerging after the earthquakes, e.g., the Structural Engineering Society of New Zealand (SESOC) and the Canterbury Earthquake Royal Commission (CERC) reports, proposed explanations to the failures observed and provided recommendations to the New Zealand Concrete Structures Standard (NZS3101:2006) [1] in an effort to promote ductile failure modes in new construction. These recommendations have been adopted and will be published in the upcoming standard amendment. Given the immediate need to address the unexpected failures, many of these recommendations were based on engineering judgement rather than research. Therefore, a large-scale experimental study is underway to assess the impact of the main changes proposed. This paper is a precursor to the experimental testing and focuses on the development of a non-linear finite element model in VecTor2 that was calibrated to results of previous tests and was then used to blindly predict the behaviour of the aforementioned specimens prior to testing.

2. Changes to NZS3101:2006 Wall Provisions

New recommendations for axial load limit and confinement detailing are discussed in this section. These and many other recommendations stem from the SESOC Interim Guidelines [2]. The full list of NZS3101:2006 amendments is currently only available in draft form.

2.1 Axial Load Limit Recommendations

An axial load limit equal to 30% of the wall compression capacity was introduced in the new amendment of NZS3101:2006:

$$N^* \leq 0.3\emptyset A_g f'_c \tag{1}$$

where N* is the design axial load at ultimate limit state, ϕ is the strength reduction factor of 0.85, A_g is the gross cross sectional wall area and f'_c is the specified concrete compressive strength. The limit was intended to reduce wall vulnerability to non-ductile compression failure with consideration of potential increases in wall axial load due to restrained elongation or beam outrigger effects in coupled walls. Through plane-strain moment-curvature analysis it is clear that axial load will increase the ultimate strength capacity and decrease the deformation capacity of a wall. Wall displacement capacity as a function of the applied axial load ratio has not been systematically studied in well-confined walls (although other studies, including [3] and [4] have studied walls with high axial load ratios and low or no confinement).

2.2 Web cross-ties and confinement

A new clause has been added to NZS3101:2006 (Cl 11.4.5.3) in the upcoming amendment, making cross-ties in the web region of the wall mandatory for 'ductile' classed walls. Currently, the use of cross-ties outside the wall end region is not common in New Zealand wall construction. The cross-ties are intended to provide anti-buckling restraint to web longitudinal bars and will inherently increase the confinement on the web concrete section. This detail is also in the process of being balloted for inclusion in the American Concrete Institute (ACI) Building Code (ACI-318-14). Aside from introducing additional fabrication costs, this detail will increase congestion of the reinforcement cage. These disadvantages may be outweighed by the benefits gained in increased ductility due to confinement of concrete and restraint against buckling of longitudinal reinforcement in the web. Tests performed by Kuang and Ho [3] on squat shear walls and Hube et al. [4] on unconfined, flexural-compression governed walls have suggested web cross-ties can improve wall displacement ductility by up to 60%.

In addition to provisions for web cross-ties, provisions for the end region confinement have been revised in the proposed NZS3101:2006 amendment. In the current version of the standard, it is permitted to only partially confine the compressive zone of the wall. In the new amendment, the confinement length is extended over the entire neutral axis depth in an effort to mitigate against the uncertainty in axial load and neutral axis depth due to wall elongation and to increase ductility and prevent compression failure. Although the effects of this change have not been tested, a database study has suggested that longer confinement lengths can lead to improved displacement capacity [5].

3. Experimental Program

To investigate the effects of axial load and the new confinement detailing on the performance of walls with ductile detailing, four one-half-scale test specimens are being tested. The cross-sections for C10-A30 are presented in Fig. 1, and the test variables are summarised in Table 1. Specimens are identified by the NZS3101:2006 version used for the design of the wall (**C**urrent or **A**mended) and the percent axial load applied (e.g., '-10' refers to $0.1A_gf'_c$). The geometry and the unconfined concrete strength (30MPa) are identical for all four specimens. In order to compare the effectiveness of confinement provided by hoops to that provided by cross-ties, an asymmetrical end region transverse reinforcement detailing has been implemented in each wall. The reinforcement grade used was either G300 (300MPa) or G500 (500MPa), with the latter identified by the letter 'H' in Fig 1. Smooth and deformed reinforcement is identified by the letters 'R' and 'D', respectively. The walls have been designed with typical detailing and geometry for an 8-storey idealized prototype building located in Wellington, New Zealand. To ensure a flexural response, capacity design principles are adopted for shear strength design, resulting in low shear demands as seen in Table 2. As only the lower two storeys of the walls have been constructed for testing, the demands from the upper six storeys including moment, shear and axial force will be applied to the top of the walls to simulate a shear span ratio of 4.6 consistent with the demands expected for the idealized prototype.

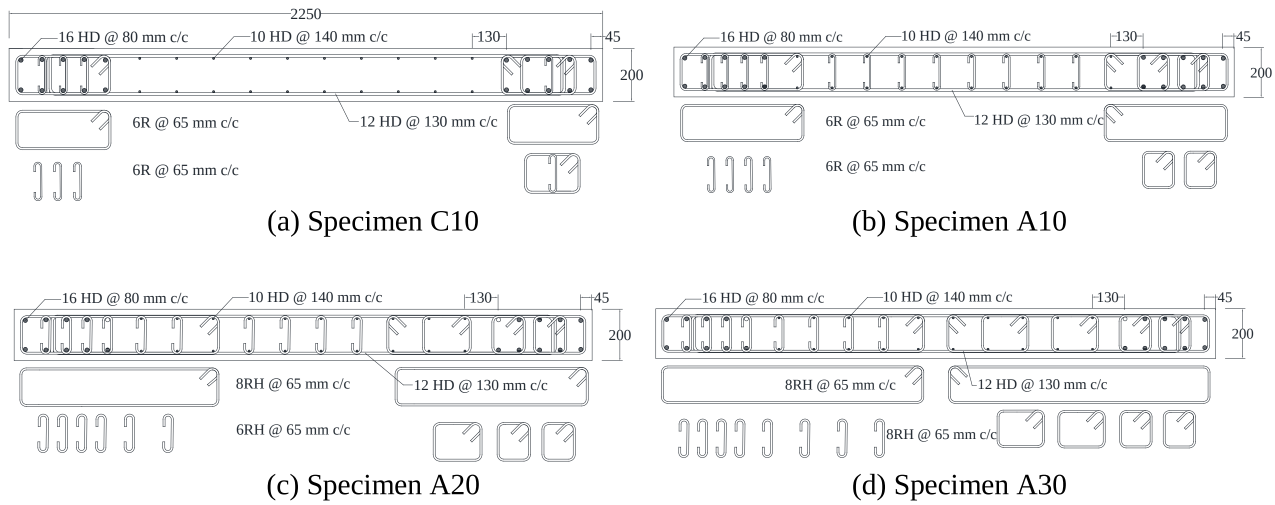

Figure 1: Cross-sections of wall specimens in the study.

Table 1 – Testing parameters of each wall specimen.

Specimen	Axial load	Web ties	Confinement length
C10	$0.1A_gf'_c$	No	Partial[(a)]
A10	$0.1A_gf'_c$	Yes	Full[(b)]
A20	$0.2A_gf'_c$	Yes	Full[(b)]
A30	$0.3A_gf'_c$	Yes	Full[(b)]

[(a)]As determined under the current version of NZS3101:2006 (2nd Amendment).
[(b)]As determined under amended version of NZS3101:2006 (3rd Amendment)

4. VecTor2 Modelling Approach

VecTor2 is a finite element software developed at the University of Toronto and is unique in implementing the Vecchio and Collins' [6] Modified Compression Field Theory. Part of a larger suite, VecTor2 was developed specifically to allow nonlinear analysis of 2D membrane-type reinforced concrete elements subjected to shear and normal stresses. A useful feature of VecTor2 is the ability to easily integrate various material behaviour models in multiple combinations, making it a very powerful tool for constituent material model comparison. A detailed explanation of VecTor2 elements and models is given in the "VecTor2 & FormWorks User's Manual: Second Edition" by Wong et al. [7].

In formulating a suitable mesh for the Vector2 model, it was necessary to divide the walls into separate regions corresponding to the heavily reinforced end regions, the lightly reinforced web and the stiff foundation and concrete top beam. In the model, all transverse reinforcement was smeared and all longitudinal reinforcement discretized. The Menegotto-Pinto [8] constitutive relationship shown in Fig. 2a was used for modelling steel reinforcement behaviour. Bauschinger effects were accounted for under cyclic loading. Reinforcement buckling was modelled through the Dhakal-Maekawa [9] model; however, the wall responses were insensitive to this formulation as ratio of stirrup spacing to the longitudinal reinforcement diameter (ranging from 3.2 to 4.0 for the walls in Fig. 1) was below the threshold of 5.0 that triggers buckling in the model. For this reason, the thin strip of cover concrete at the wall edge was deemed to no longer have significance on the wall performance and in order to save on computational demand, was modelled with identical properties to the rest of the end region.

The concrete material stress-strain behaviour and confinement effects were important factors to consider in the model as the specimens used for calibration all failed in either crushing or simultaneous crushing and reinforcement buckling. The Hognestad parabola [10] and the Mander et al. [11] models were used to model pre- and post-peak concrete response, respectively. In the validation of the model, it was found that the default confinement model resulted in accurate prediction of the ultimate strength capacity, and an overestimation of the deformation capacity. A prediction for the wall deformation capacity was achieved by using manually-calculated peak confined concrete stress (f'_{cc}) and strain (e_{co}) values (based on rectangular sections, consistent with the approach of Mander et al.[11]) and modelling the post-peak response as an unconfined material. The resulting material model is presented in Fig. 2b. This approach was adopted based on evidence from recent tests on compression-governed walls [12] and boundary element prisms [13] suggesting that confined concrete does not exhibit the idealised, well-spread post-peak ductility in compression failures. Instead, failure is localised and crushing occurs immediately after peak strength capacity is reached.

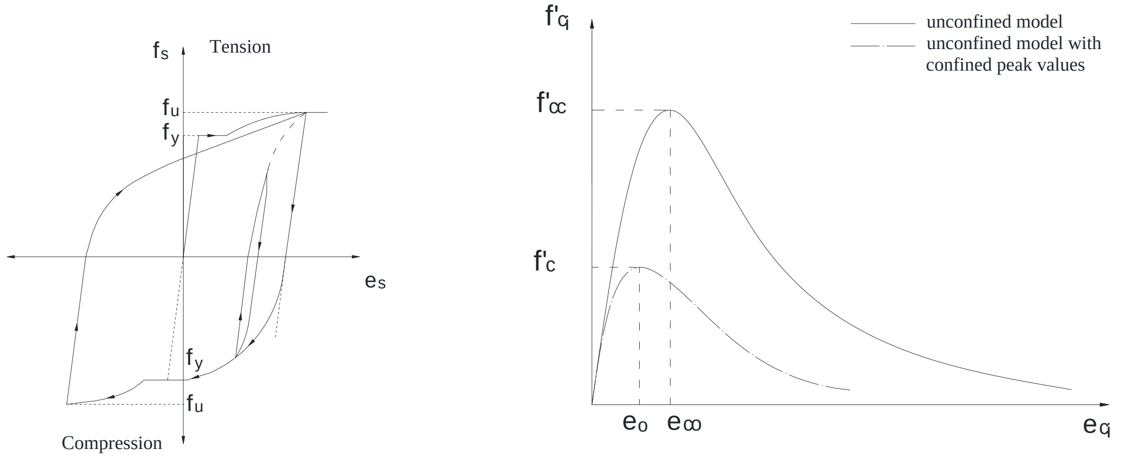

(a) Menegotto-Pinto w/ Bauschinger effects (b) Mander et al. unconfined concrete model

Figure 2: Material models adopted in VecTor2 analysis.

Simulations with a range of mesh characteristics indicated that the response near failure was highly dependent on element size due to localized failure, characterized by significant element distortion of the critical corner wall elements. This is a well-known modelling issue for softening-type failures and is normally overcome through material regularization using concrete inelastic fracture energy methods [14]; however, given the closed-source nature of VecTor2, this procedure was not possible. Pugh [15] has previously acknowledged this VecTor2 shortcoming; however, no further modelling approaches have been proposed to address this issue. In this study it was determined that an element size of 100 mm yielded reliable results across the range of the experimental tests modelled.

5. Calibration of Model

Nonlinear finite element models were created in the VecTor2 software and were calibrated to a set of tests chosen from the University of Auckland RC wall database [5] that possess reinforcement detailing, applied loading, and likely failure mode similar to C10-A30. The cross-sections for these calibration specimens are shown in Fig. 3 and additional specimen characteristics are summarised in Table 2. Load-deformation results from the models and tests are shown in Fig. 4. Cycles at small elastic drifts and repetitions of cycles at the same drift have been omitted from the figures for clarity. Note that due to the nature of numerical convergence in VecTor2, the prescribed cycle drifts were not always precisely achieved. Model results for peak base shear (V_p), drift at peak base shear (Δ_p), and drift at failure (Δ_u) (defined as drift at which crushing of the wall is first observed) are compared with measured values in Table 3

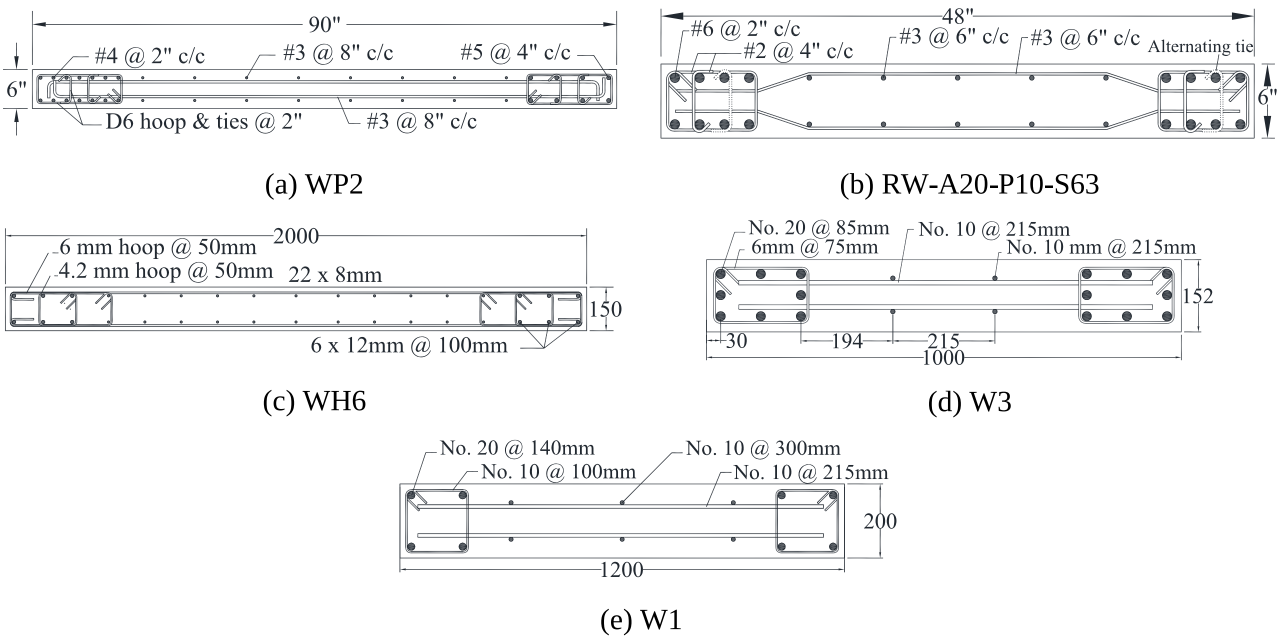

Figure 3: Cross-sections of specimens used for validation of the VecTor2 modelling approach.

Table 2 – Reinforcement and loading characteristics of simulated walls.

Study	Wall	Axial load	Shear-span ratio	ρ_{IE} (a)	Shear demand(b)
Shegay et al.	**C10-A30**	**0.1-0.3$A_g f'_c$**	**4.6**	**2.8**	**2.2-2.9**
Segura & Wallace (2015)	WP2	0.1$A_g f'_c$	3.8	2.8	2.5
Tran (2012)	RW-A20-P10-S63	0.07$A_g f'_c$	2.0	7.1	6.1
Dazio et al. (2009)	WH6	0.11$A_g f'_c$	2.6	1.5	2.5
Cho et al. (2004)	W3	0.1$A_g f'_c$	3.8	6.3	4.3
Liu (2004)	W1	0.08A_g'f_c	3.1	3.0	2.4

(a)Longitudinal reinforcement ratio in the wall end region.

(b)Defined as $V_p/A_g\sqrt{f'_c}$ (psi).

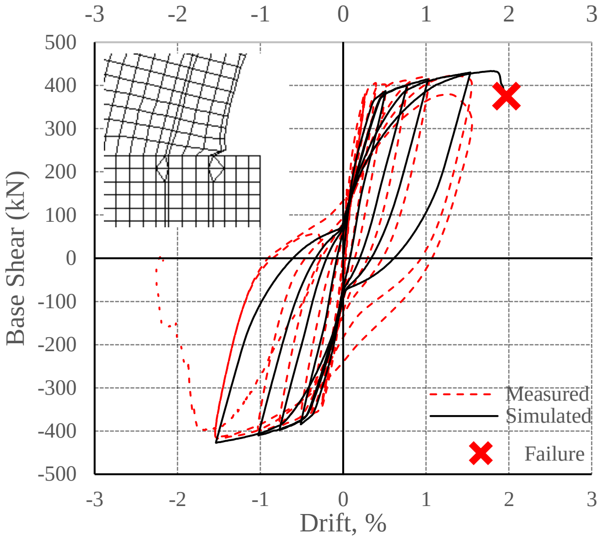

(a) WP2

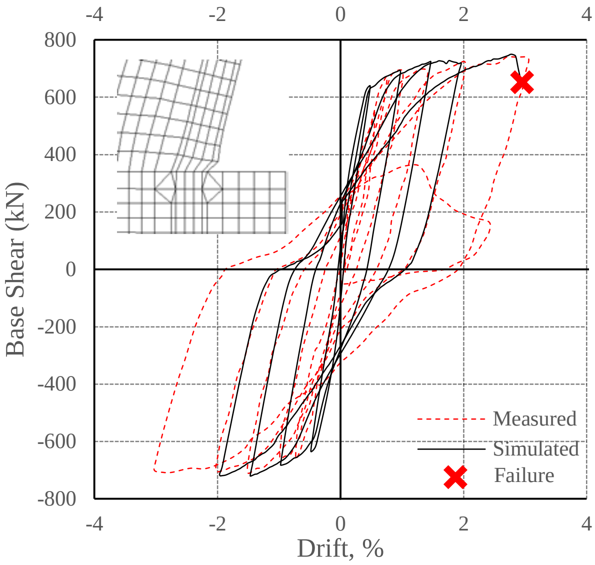

(b) RW-A20-P10-S63

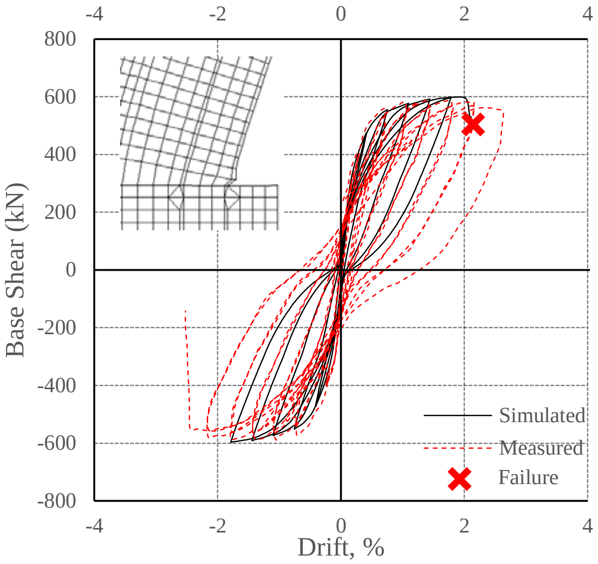

(c) WH6

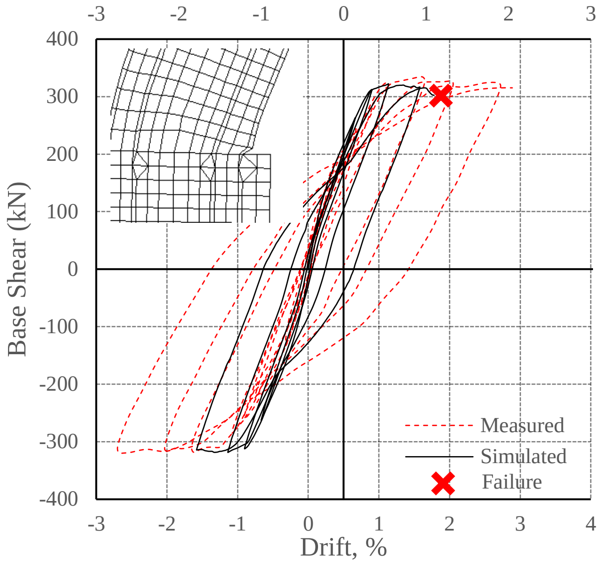

(d) W3

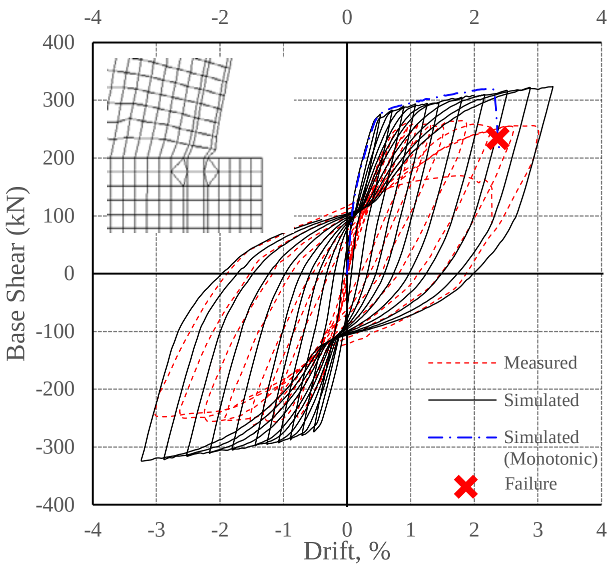

(e) W1

(f) Typical crushing failure in wall tests [16]

Figure 4: Comparison of VecTor2 models to experimental data.

Table 3 –Comparison of test results and model results.

	Peak Base Shear, V_p (kN)			**Drift t at peak base shear, Δ_p**			**Drift at failure, Δ_u**		
Specimen	Exp.	Model	Exp/Model	Exp.	Model	Exp/Model	Exp.	Model	Exp/Model
WP2	413	430	0.96	1.7	1.8	0.94	1.7	1.8	0.94
RW-A20-P10-S63	740	742	1.0	3.0	2.8	1.07	3.0	2.8	1.07
WH6	597	589	1.01	2.1	2.0	1.05	2.6	2.0	1.3
W3	335	330	1.02	1.7	1.7	1.0	3.0	1.7	1.8
*W1	266	317	0.84	1.8	2.3*	0.78	3.0	2.3*	1.3

*Observed from monotonic results

In Fig. 4, model results matched the peak cycle loads at each drift with good accuracy, adequately capturing the strain hardening effects where present. Peak base shear is simulated within 6% for all specimens but W1 (see Table 3). The simulated initial stiffness of the walls is generally close to the measured response and is particularly accurate for specimen WH6. Stiffness degradation in ascending cycles is captured well in all of the models. The unloading behaviour is simulated with good accuracy for all specimens up until lower base shears are reached. As the walls are cycled back through 0kN base shear, the hysteresis exhibits a pronounced pinching effect as seen in the simulated response of specimens WP2 and WH6. This effect is the result of under estimation of stresses carried by the compression reinforcement within open cracks.

Simulating the failure mode and the corresponding drift at which this happens was a necessary step in the calibration process to then be able to predict the failure characteristics of specimens C10-A30. The five calibration specimens all lost capacity in a crushing-type failure model as representatively shown in Fig. 4f. In VecTor2, crushing of concrete is seen as a localization of deformations in the corner elements on the wall, as shown on each plot in Fig. 4. In the hysteresis curve, the localization corresponds to a sudden and distinct drop in section strength, characterised by a negative slope, followed by poor numerical convergence. The monotonic backbones showed this clearer, as exemplified in Fig. 4e. This initial drop was defined as failure of the section and the analysis was terminated, despite capability of the simulated section to sustain additional deformation past this point. Experimental results show that this definition is appropriate, as failure of the section is often described to occur almost immediately after crushing of core concrete is first observed. Using this definition of failure, the drift at which the walls failed in crushing was simulated within 10% walls WP and RW-A20-P10-S63, within 30% for walls WH6 and W1 and poorly predicted for W3 as shown in Table 3.

6. Blind Predictions of C10-A30

The VecTor2 model was used to make blind response predictions of walls C10-A30 in an effort to capture the effects of changes in confinement detailing between C10 and A10 and changes in axial load between A10, A20 and A30 on load-deformation response. For all walls, the same, reversed-cyclic loading protocol was adopted. One cycle was completed at drifts of 0.5%, 1.0%, 1.5%, 2.0%, 2.5%, and 3.0%, unless failure occurred earlier. Small cycles below 0.5% drift were excluded in the protocol. Results of the reverse cyclic simulations for specimens C10-A30 are presented in Fig. 5. Table 4 summarises the peak base shear (V_p), the drift corresponding to peak base shear (δ_p), the drift at first reinforcement yield (δ_y) and the drift at failure (δ_u), where drift is the lateral displacement of the wall at full height normalized by the full wall height.

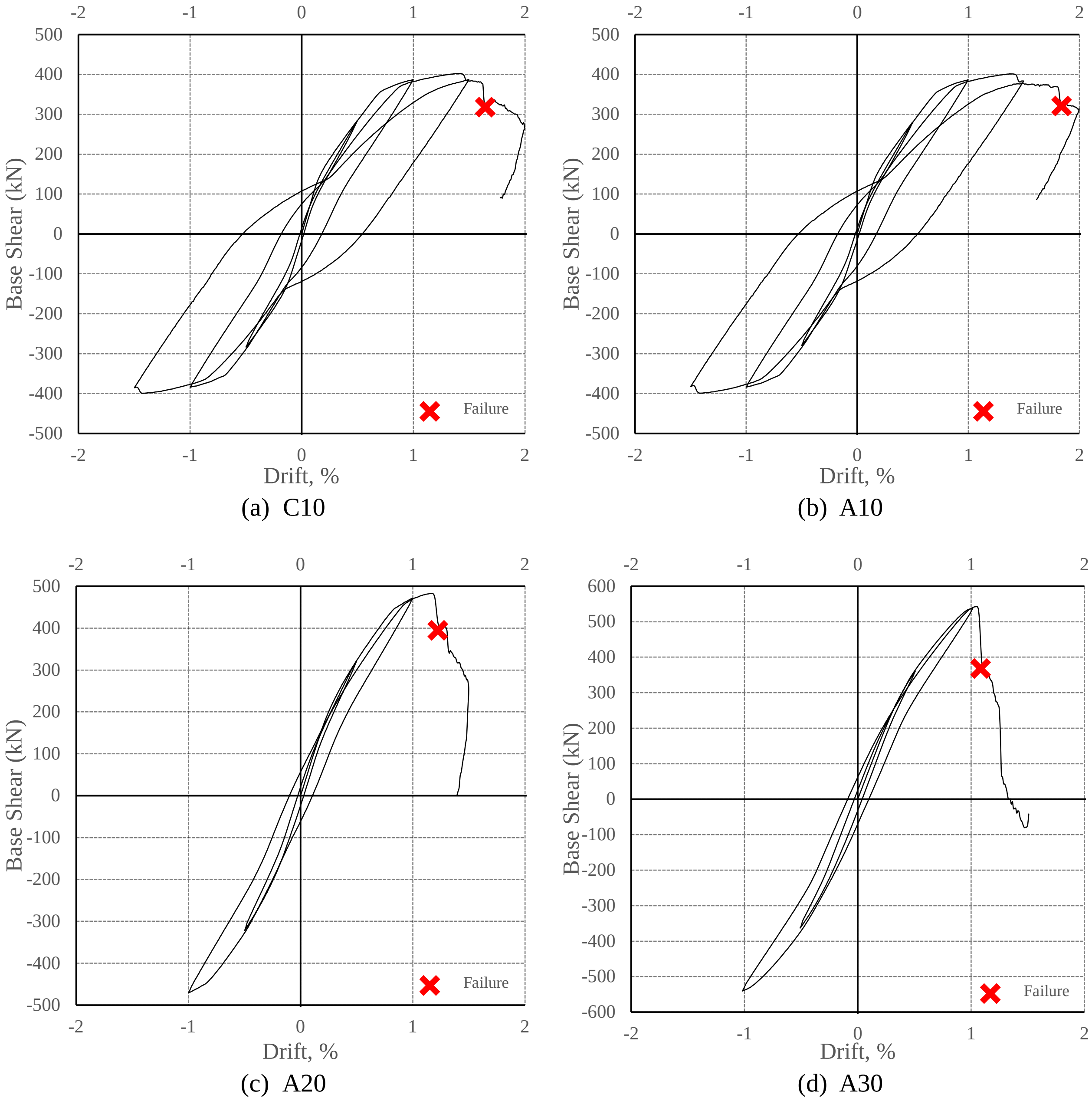

Figure 5: Load-deformation curves as predicted by VecTor2 for C10-A30.

Table 4 – Peak drift and base shear values for VecTor2 from analysis of C10-A30

Wall	**Axial Load**	V_p[a], **kN**	δ_p[b]	δ_y[c]	δ_u[d]	**Displacement ductility**[e], δ_u/δ_y	**Peak tensile strain**[f], **mε**
C10	$0.1A_gf'_c$	402	1.47	0.69	1.6	2.9	3.3
A10	$0.1A_gf'_c$	401	1.43	0.64	1.8	3.13	3.1
A20	$0.2A_gf'_c$	483	1.20	1.0	1.30	1.3	2.8
A30	$0.3A_gf'_c$	543	1.05	1.05	1.05	1.0	2.7

[a]Peak shear occurring at the base of the wall.
[b]Drift at which peak base shear is recorded.
[c]Drift at which longitudinal reinforcement first yields in the model.
[d]Drift at which crushing (and therefore failure) is first observed.
[e]The drift at crushing normalized by drift at first reinforcement yield.
[f]Maximum average strain attained in tension reinforcement before specimen failure.

It is evident from the results shown in Table 4 that an increase in wall axial load leads to an increase in lateral load carrying capacity, an increase in stiffness, and a decrease in the drift at peak strength, all of which is expected. Capacity design has ensured a flexural response, evident by the low magnitude of peak base shears compared to section shear strength capacity (1900 kN). Failure of all four specimens is predicted to occur by crushing of the end region (Fig. 6a). In the VecTor2 post-processor, the vertical concrete strain profile indicates that compressive strains are localized to a short height of the wall (<200mm) and failure initiates in the bottom one to two elements (Fig. 6b). Localisation effects observed here are representative of some of the crushing damage observed in Christchurch as well as what has been consistently observed in compression failures in wall tests [12], [17], [18] and wall boundary element prism tests [13].

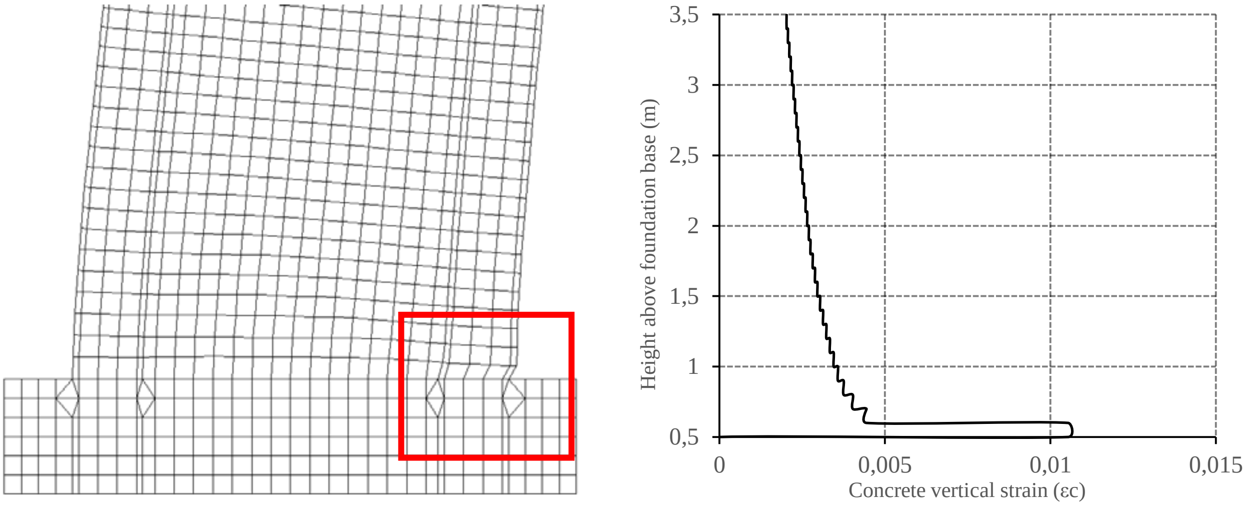

(a) localised crushing in critical corner elements (b) strain distribution up the height of the wall

Figure 6: Deformation and strain characteristics observed for all four walls at failure.

Overall, for the ductile detailing provided in the four walls, the predicted displacement ductility is less than what has been observed in previous ductile wall research [5]. Specimens C10 and A10 in Fig. 5a and 5b, respectively, display a low displacement ductility of around 3. . Brittle failure, characterized by immediate strength loss, occurs due to crushing of concrete at the wall end region at 1.6% for C10 and at 1.8% for A10 as seen in Table 4. It is possible that the higher deformation capacity of A10 is attributed to the improved end region and web confinement detailing as proposed in the new NZS3101:2006 amendment. However, this is difficult to know for certain as the highly localised failure mode appears to be independent of these variables. Specimens A20 and A30 in Fig. 5c and 5d, respectively, exhibit effectively no displacement ductility. Despite similar average peak reinforcement strains in all walls as shown in Table 4, A20 and A30 develop cracks over a shorter wall height above the base of the wall that leads to less localised strains and a nearly-elastic response with negligible energy dissipation and immediate strength loss at failure. A20 and A30 failed in compression at low drifts (1.3% and 1.05%, respectively) after the same number of cycles due to the high axial load. The crushing failure occurs when inelastic strains in the tensile reinforcement are small (approximately 0.28% or $1.1\varepsilon_y$, where ε_y is the yield strain). Additional axial load in excess of $0.2A_g f'_c$, as for A30, did not change the wall performance after δ_y.

These predictive results suggest an inadequacy of the $0.3A_g f'_c$ axial load limit to maintain the ductile performance of walls. For gravity load bearing, uncoupled RC walls, the new limit would almost never be reached in design. However, coupled walls are especially prone to the undesired failures simulated as axial load can easily reach $0.3A_g f'_c$ due to beam coupling action. These results will be confirmed through the large-scale test program described.

7. Conclusions

A study is underway at the University of Auckland to investigate the effects of proposed amendments to NZS3101:2006 relating to RC wall axial load limitations and extended confinement detailing, on wall response. This study includes large-scale testing of four specimens (C10-A30) with varying confinement detailing and applied axial loads. Predictions of the experimental results for C10-A30 are made in the

VecTor2 finite element software based on a modelling approach calibrated to four previously-conducted tests with similar parameters to C10-A30. The following conclusions were drawn from this study:

- For the four specimens used for calibration, model results were in good agreement with test results in terms of peak strength capacity and initial stiffness. The hysteretic curve was adequately simulated in the loading branches but the degree of pinching during unloading was overestimated by the model (i.e., more pinching for the model) for two of the five walls. The VecTor2 modelling approach was used to consistently predict the flexural compression failure mode while the drift at failure was predicted within 10-30% accuracy on average.

- Simulations run with VecTor2 were used to predict similar response for C10 and A10, governed by a crushing failure at a drift of 1.6% and 1.8%, respectively. The improved end region and web confinement detailing implemented in A10 suggest a minimal increase in deformation capacity; however, this will need to be confirmed through experimental results as the localised failure model appeared to be independent of the amended detailing. The predicted ductilities for each specimen are low compared what has previously been observed in ductile wall test.

- Specimen A20, with an axial load of $0.2A_gf'_c$, was predicted to experience non-ductile failure at 1.3%, with lower predicted drift at failure than for C10 and A10. The crushing failure was simulated to occur before cracks and tensile yielding could spread over the plastic hinge length, thus no appreciable ductility and energy dissipation occurred prior to failure. The hysteretic behaviour of A30 did not differ significantly from A20 despite the substantial increase in axial load to $0.3A_gf'_c$.

- It is evident from the numerical results of the Vector2 modelling that concrete crushing preceding failure occurs over a very short distance above the base of the wall in the end region. The strain profile up the height of the wall confirmed that compressive strains had concentrated at the base of the wall. Whether this localisation is an accurate representation of the wall response or a characteristic of VecTor2 formulation will be determined in experimental tests in August 2016.

8. References

[1] Standards New Zealand, (2012): *NZS 3101:2006 Concrete Structures Standard Part 1 - The Design of Concrete Structures (Amendment 2)*. Wellington, New Zealand.

[2] SESOC, (2013): Interim Design Guidance: Design of Conventional Structural Systems Following the Canterbury Earthquakes.

[3] Kuang JS and Ho YB, (2009): Seismic Behavior and Ductility of Squat Reinforced Concrete Shear Walls with Nonseismic Detailing. *ACI Structural Journal*, **2**(105), 225–232.

[4] Hube MA, Marihuén A, de la Llera JC, and Stojadinovic B, (2014): Seismic behavior of slender reinforced concrete walls. *Engineering Structures*, **80** 377–388.

[5] Shegay AV, Motter CJ, Henry RS, and Elwood KJ, (2015): A database for investigating NZS3101 structural wall provisions. *Pacific Conference on Earthquake Engineering*, Sydney, Australia.

[6] Vecchio FJ and Collins MP, (1986): The modified compression-field theory for reinforced concrete elements subjected to shear. *ACI Journal Proceedings*, **83**(2), 219–231.

[7] Wong PS, Vecchio FJ, and Trommels H, (2002): VecTor2 & FormWorks User's Manual: Second Edition. Toronto.

[8] Menegotto M and Pinto PE, (1973): Method of Analysis for Cyclically Loaded R. C. Plane Frames Including Changes in Geometry and Non-Elastic Behavior of Elements under Combined Normal Force and Bending. Rome, Italy.

[9] Dhakal RP and Maekawa K, (2002): Modeling for Postyield Buckling of Reinforcement. *Journal of Structural Engineering*, **128**(9), 1139–1147.

[10] Hognestad E, (1951): A Study of Combined Bending and Axial Load in Reinforced Concrete Members. Urbana-Champaign, IL.

[11] Mander JB, Priestley MJN, and Park R, (1988): Theoretical Stress-Strain Model for Confined Concrete. *Journal of Structural Engineering*, **114**(8), 1804–1826.

[12] Segura C and Wallace J, (2015): Experimental Study on the Seismic Performance of Thin Reinforced Concrete Structural Walls. *Structural Engineering Frontier Conference Proceedings 2015*, Yokohama, Japan.

[13] Arteta AC, (2015): Seismic Response Assessment of Thin Boundary Elements of Special Concrete Shear Walls., University of California, Berkeley.

[14] Coleman J and Spacone E, (2001): Localization Issues in Force-Based Frame Elements. *Journal of Structural Engineering*, **127**(11), 1257–1265.

[15] Pugh JS, (2012): Numerical Simulation of Walls and Seismic Design Recommendations for Walled Buildings., University of Washington.

[16] Tran TA, (2012): Experimental and Analytical Studies of Moderate Aspect Ratio Reinforced Concrete Structural Walls., University of California, Los Angeles.

[17] Dazio A, Beyer K, and Bachmann H, (2009): Quasi-static cyclic tests and plastic hinge analysis of RC structural walls. *Engineering Structures*, **31**(7), 1556–1571.

[18] Thomsen IV HJ and Wallace JW, (1995): Displacement-Based Design of RC Structural Walls: An Experimental Investigation of Walls with Rectangular and T-Shaped Cross-Sections. Potsdam, New York.